Appl. Phys. B 85, 31–44 (2006)
DOI: 10.1007/s00340-006-2400-1

Applied Physics B
Lasers and Optics

G. WILPERS*
C.W. OATES✉
L. HOLLBERG

Improved uncertainty budget for optical frequency measurements with microkelvin neutral atoms: Results for a high-stability ^{40}Ca optical frequency standard

Time and Frequency Division, National Institute of Standards and Technology, 325 Broadway, Boulder, CO 80305. USA

Received: 9 January 2006/Revised version: 29 June 2006
Published online: 17 August 2006 •

ABSTRACT Using a Ca optical frequency standard at 657 nm, we demonstrate a method that reduces uncertainties in absolute frequency measurements of optical transitions using freely expanding neutral atoms. Working with atoms that have been laser cooled to 10 μK, we have developed and employed a new technique that combines launching of cold atom clouds with atom interferometry to measure and optimise spectroscopy beam parameters. When applied to a frequency standard with laser beams of high spatial quality, this approach can potentially reduce residual Doppler effect uncertainties to well below one part in 10^{16}. With Doppler uncertainties greatly suppressed, we investigate other potential shifts at the 1-Hz level with a multiplexed measurement system that takes advantage of the low instability of the calcium frequency standard (4×10^{-15} at 1 s). The resultant fractional frequency uncertainty for the standard is 6.6×10^{-15}, the lowest uncertainty reported to date for a neutral atom optical standard.

PACS 06.30.Ft; 32.30.-r; 39.20.+q

Introduction

In recent years there has been a dramatic surge of interest in optical frequency metrology, in part due to advanced laser cooling methods and the widespread implementation of femtosecond-laser-based frequency combs, which enable direct connection between the optical and countable microwave domains [1–5]. The most accurately known optical frequencies are those of transitions in single ions, which have now been measured with fractional frequency uncertainties approaching one part in 10^{15} [6–8]. While lattice-based systems look extremely promising [9], the most accurate frequency measurements of neutral atom transitions currently use clouds of laser-cooled atoms that are allowed to expand freely in the Earth's gravitational field [10–12]. Such systems can have high signal-to-noise ratios (SNRs) due to the large numbers of atoms involved (10^6 or more), but atom motion can lead to significant Doppler-related uncertainties (unlike their trapped-ion counterparts, which have no first-order Doppler effect due to the ions being in the Lamb–Dicke regime). Recent advances in laser cooling have led to temperatures near the recoil limit for atomic samples used in optical frequency standards [13–17]. Already groups are beginning to enjoy the benefits of reduced temperatures to achieve smaller uncertainties for measurements of neutral atom transitions [18, 19].

Now that temperatures for suitable optical clock atoms are nearing their expected cooling limits (~ 1 μK), it is timely to consider how well transition frequencies can really be measured in the laboratory with freely expanding cold atoms, and to identify potential limitations [20]. Here we demonstrate how to use the colder atom temperatures to achieve a fractional transition frequency uncertainty of less than 10^{-14} with excellent prospects for considerable improvement. First, we describe a new technique that takes advantage of the microkelvin atoms to improve the spatial wave front characteristics of the laser beams themselves, since laser cooling alone does not reduce the residual first-order Doppler uncertainty to a negligible level. This method, which uses atom interferometry with launched clouds of cold atoms to improve probe laser beam parameters (e.g. wave-front flatness and mutual beam tilt), could reduce Doppler uncertainties to below 50 mHz (10^{-16} fractionally) for beams of high spatial quality. Second, with first-order Doppler uncertainties contributing less than 1 Hz in our current apparatus, we present a detailed investigation of other potentially significant physical and technical effects at the hertz level. This evaluation of potential shifts was greatly expedited by an interlaced measurement system designed to take advantage of the low fractional frequency instability (4×10^{-15} at 1 s) of the clock apparatus. Finally, we report a total fractional uncertainty for the Ca frequency standard of 6.6×10^{-15}, which is the lowest uncertainty to date reported for a neutral optical frequency standard. Since the largest contributors to the uncertainty are technical in nature, prospects for improvement by an order of magnitude (or more) look promising.

2 Experimental apparatus

2.1 *Overview*

The principal experimental setup has been described in detail in earlier publications [10, 17, 21, 22], but

✉ Fax: +1-303-497-7845, E-mail: oates@boulder.nist.gov
*Present address: National Physical Laboratory, Teddington, Middlesex, TW11 0LW, UK

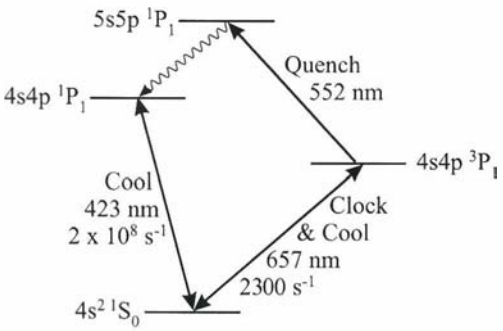

FIGURE 1 Partial energy-level scheme for neutral ^{40}Ca, showing transitions relevant to the Ca optical frequency standard

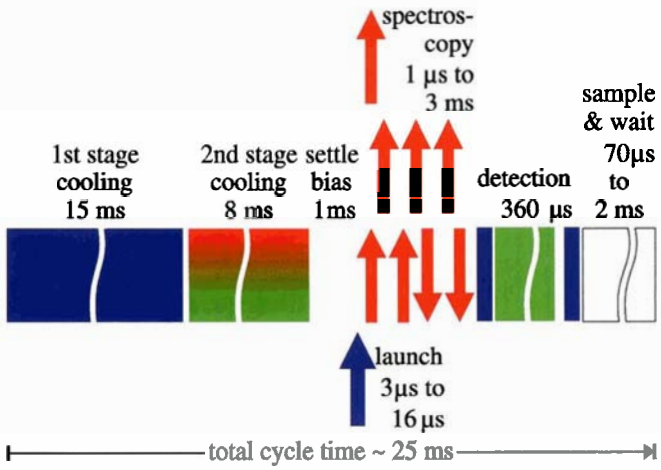

FIGURE 2 The cycle used to perform the spectroscopic measurements described in this work. First-stage cooling is used to collect atoms and cool them to 2 mK. The second stage of cooling uses the narrow 657-nm transition in combination with the 552-nm quenching transition to reduce the atom temperature to ~ 10 µK. After optional launching pulses that are used in some systematic investigations, the clock spectroscopy sequence occurs, followed by normalised 423-nm detection pulses. An optional delay can be added at the end to test for synchronised systematics. See text for details

here we summarise the apparatus with particular emphasis on the aspects most relevant to the reduction of the clock frequency uncertainties. The 657-nm intercombination line (see Fig. 1) in neutral ^{40}Ca has been the subject of atom interferometric and precision spectroscopic studies for over thirty years, due to its nearly ideal realisation of a closed two-level system with a long coherence time (natural line width = 375 Hz [18]). The $m = 0 \rightarrow m = 0$ transition is highly insensitive to external magnetic and electric fields and has shown no evidence to date of collisional shifts at the 10^{-15} level [10], making it an excellent candidate for an optical frequency standard. This transition is one of the recommended radiations for the realisation of the metre and has been the subject of absolute frequency measurements for nearly a decade at the Physikalisch Technische Bundesanstalt (PTB) and the National Institute of Standards and Technology (NIST) [2, 10, 18]. The uncertainty with which this transition frequency has been measured has been reduced by several orders of magnitude in the last few years, due in part to improved stabilisation of the probe lasers, but due mainly to advances in laser cooling, which greatly reduce the Doppler uncertainties in finding the unperturbed transition frequency [10, 18].

Our experiment uses two stages of laser cooling to reduce the temperature of the atomic sample to ~ 10 µK. Since the laser cooling beams shift the levels involved in the clock transition, they are turned off during the clock spectroscopy. This leads to a measurement cycle that consists of an atom preparation period and a clock transition spectroscopic period. In order to improve the clock stability (see Sect. 3), we have designed the apparatus to have the shortest measurement cycle (< 25 ms) that will not compromise the measurement accuracy. The cycle time is presently limited by the need to reload the trap and achieve a narrow velocity distribution in the second-stage cooling (Sect. 2.2).

2.2 *Cooling apparatus*

The measurement cycle is depicted in Fig. 2. It commences with the first stage of laser cooling, during which we use the strong transition at 423 nm (see Fig. 1 for relevant energy levels) to load atoms from an atomic beam into a standard six-beam magneto-optic trap (MOT). Through frequency doubling of a semiconductor laser system, we generate about 40 mW of 423-nm cooling light. This light is sent through several acousto-optic modulators (AOMs) to shift the frequencies of the various beams to the appropriate detunings. To achieve fast shut-off with a large extinction ratio to minimise Stark shifts (see Sect. 5.2.1), a minimum of three AOM stages is used for each beam. The first two AOM stages actually consist of a single double-pass AOM that is also used to stabilise the intensity (< 20 µs settling time for switching on) of the 423-nm light. Although we do not use a Zeeman slower coil, a counterpropagating 423-nm beam detuned by −245 MHz decelerates slow atoms (initial velocity below 100 m/s) from a thermal beam, thereby increasing the loading rate of atoms by a factor of more than 10. For simplicity, the present version of the apparatus does not use a repumping beam at 672 nm to close a leak to the metastable D state from the excited state of the broad Doppler cooling transition [21, 23]. During a 15-ms loading period the trap is filled with ~ 5×10^6 atoms at a temperature of ~ 2 mK, which is within a factor of three of the Doppler limit.

More than 20% of these atoms are then cooled to ~ 10 µK with a three-dimensional, second stage of quenched cooling [15–17] using the 657-nm clock transition in conjunction with a repumping transition at 552 nm [17]. The light for this second-stage cooling is controlled by AOMs with extinction ratios leading to negligible levels of leakage light during the clock transition spectroscopy (Sect. 5.2.1). The second-stage cooling period lasts only 7 ms, and operates without an applied magnetic quadrupole field. During this time, however, the extinguished MOT quadrupole field (0.6 T/m) decays, yielding a background field of less than 0.5 µT at the end of the second-stage molasses. We measure the atom temperature (along with drift velocities) in three orthogonal dimensions using the narrow clock transition (see Fig. 3). Within the 7 ms of second-stage cooling a narrow Gaussian velocity distribution with low offset velocities can be achieved that allows one to minimise the residual Doppler effect (Sect. 4).

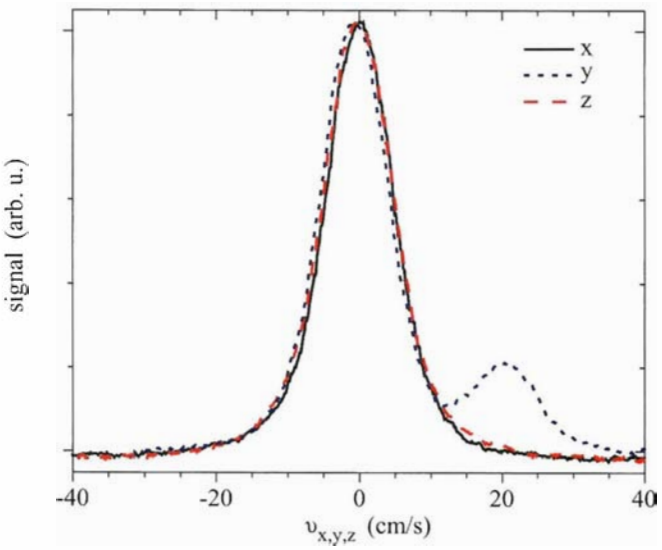

FIGURE 3 The atomic velocity distribution measured in all three dimensions after 15 ms of first-stage cooling and 7 ms of second-stage cooling. The distributions are measured by scanning the frequency of the clock laser and using π pulses of 10-μs duration. For the vertical direction ('y' in the figure), the measurement can be contaminated by a back reflection from a detection lens, which causes an effective weak standing wave. To separate the contributions, we take distributions after a 11-ms delay. Gravitational acceleration during this delay leads to a large drift velocity (10.8 cm/s), which resolves the two contributions via the opposite signs of their Doppler shifts. In practice, typical velocity offset values for the three directions were less than 1.1 cm/s

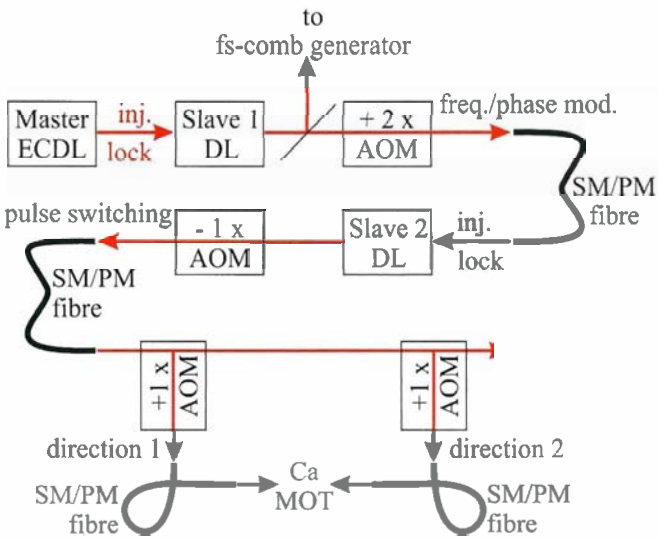

FIGURE 4 The apparatus used to generate red probe pulses. The frequency-stabilised master diode laser (DL) in external-cavity configuration (ECDL) controls slave laser 1, which in turn controls slave laser 2. A double-pass acousto-optic modulator (AOM) between the lasers enables precise modulation of the probe frequency and phase. Injection-locked laser 2 sends light through an AOM that generates the probe pulses before passing through a fibre for equal pulse shaping for all probe directions. Finally, the red light passes through AOMs that direct the light through either of two single-mode, polarisation-maintaining (SM/PM) fibres for spatial filtering before collimation for the Ca spectroscopy

2.3 *Probe laser apparatus*

We excite the clock transition in a variety of ways through the use of different probe pulse sequences in the time domain. Single pulses are used to measure Rabi-flopping rates or velocity distributions while three- and four-pulse atom interferometers are used to measure systematic frequency shifts or stabilise the clock laser to calcium (see Sect. 2.4 and Fig. 2 for details). To achieve highest resolutions with low noise levels, it is necessary to have a laser with a very narrow line width. To this end, we lock the frequency of an extended-cavity diode laser (with a good anti-reflection coating) to a narrow resonance ($\Delta\nu = 9$ kHz) of an environmentally isolated Fabry–Pérot reference cavity. This cavity rests on a floating table with active tilt control, and is enclosed in a thermally controlled, vibrationally isolated vacuum chamber [21]. Measurements via a femtosecond laser that is locked to an extremely stable reference laser at 563 nm (used in the $^{199}Hg^{+}$ frequency standard at NIST [24]) provide an upper limit to the probe laser line width of 2 Hz in a 1-s measurement period [25]. Frequency tuning of the laser relative to the cavity is achieved with a maser-referenced synthesiser. The rf output drives a double-pass AOM to control an offset between the laser and the reference cavity. The frequency-offset laser light from the AOM is sent via a fibre that maintains the light polarisation and is coupled into the reference cavity.

We generate the probe pulses for the clock transition by sending rf pulses to AOMs that deflect light to optical fibres. To reduce the effects of directional switching, frequency modulation, and pulsing on the pulse spectral and spatial content, we implemented the probe beam apparatus shown in Fig. 4. The stabilised master laser provides 3 to 4 mW of power for injection locking a second laser (slave 1 in Fig. 4), which sends the majority of its light to the femtosecond comb. Additionally, this second laser provides light for injection locking a third laser (slave 2), which generates the light used for probing the atoms. The light from slave 1 is offset by an AOM in double-pass configuration and fed through a fibre before injection locking slave 2. The frequency and phase of this laser can then be controlled via the rf signal going to this offset AOM, with minimal impact on the amplitude and direction of the light that actually probes the atoms. All AOMs used in the probe laser apparatus are driven by maser-referenced synthesisers.

To provide equal pulse shapes from both probe directions, the light from slave 2 passes through a pulsing AOM that is used to generate the probe pulses and is coupled into a polarisation-maintaining optical fibre. The emergent light pulses are then coupled by directional AOMs to one or the other of the two fibres downstream that illuminate the atomic cloud. The fibres provide spatial filtering for the beams from the two directions. The directional AOMs are opened (closed) 2 ms before (after) the probe pulses are generated in the switching AOM. These time windows remove the effect of the transfer function of the directional AOMs on the pulse shapes. At the same time, the combination of laser light frequency offsets and the two-stage switching off of the probe light provides a high degree of suppression of AC Stark shifts (see Sect. 5.2.1).

2.4 *Spectroscopy on the clock transition and locking scheme*

The probe light emerging from the fibres (about 6.7-mW power in each beam) located after the directional AOMs is carefully collimated and aligned using two identical

telescope setups. They consist of a high-quality microscope objective (NA 0.55) and a plano-convex lens ($f = 200$ mm, diameter 50 mm) on micrometer stages to allow for fine adjustment of the beam diameter (~ 5.9 mm) and collimation at the position of the atoms ($\sim$ 1-m distance). The alignment procedure is outlined in Sect. 4. Prior to the spectroscopic sequence, a small magnetic bias field is turned on (parallel to the probe light electric field) to enable selective excitation of the $m = 0 \rightarrow m = 0$ transition. After a delay of 1 ms during which the magnetic field reaches its set value of $\sim 150\,\mu$T, the clock spectroscopy is performed. The spectroscopy is immediately followed by detection pulses that, with an electron shelving scheme using near-resonant light at 423 nm, measure the degree of excitation induced by the probe laser. In principle, this detection scheme can reach a SNR sufficient to enable spectroscopic performance limited only by quantum-projection noise (QPN) [22, 26, 27]. As shown in Fig. 2, this scheme uses one blue pulse directly after the spectroscopy (but before significant decay occurs) to measure the depleted ground state population. Induced fluorescence is imaged on a photomultiplier. A second pulse measures the total atom population after the excited-state population is returned to the ground state through decay and optical pumping using 552-nm light. The normalised excitation is stored and the measurement cycle is then repeated with a new frequency value for the probe laser, as desired.

For the majority of the optical clock work, we use a Bordé–Ramsey-type atom interferometer (AI) [28, 29] in the time domain, which consists of four pulses of duration T_p. The Bordé–Ramsey sequence uses frequency-stabilised 657-nm light to make a frequency-sensitive asymmetric AI. With this technique we first illuminate the atoms with a pair of time-separated pulses (time interval = T) from one direction, followed by an identical pair from the opposite direction (the time between pairs $T' = 10$ ms). As we expect with a Ramsey technique, the spectroscopic resolution depends on the time separation for each pair of pulses (the FWHM line width or resolution is $\sim 1/(4(T + T_p))$). The pulse durations were $T_p = 3$ ms, while the separations ranged from $T = 18.6$ ms to 1512 ms depending on the resolution desired. The Bordé–Ramsey approach effectively cancels the first-order Doppler shift, thereby enabling high-resolution signals to be obtained, while still allowing a large fraction of the atoms to contribute to the signal and hence ensure a good signal-to-noise ratio.

In Fig. 5, we show typical four-pulse AI spectra taken at low resolution (fringe width = 11.55 kHz). Note that due to the narrow residual Doppler width (150 kHz FWHM) of the cold atom cloud, the spectrum is Fourier-transform limited, with virtually all atoms contributing in a similar way to the observed line shape. In the low-resolution spectrum the asymmetry in the envelope containing the fringe pattern is clearly visible. This is a direct consequence of atomic recoil effects [30], and possible associated frequency shifts are discussed in Sect. 5.1.

In order to stabilise the probe laser frequency to the Ca spectroscopic signal, we modulate the laser frequency from cycle to cycle between two values separated by the fringe width. To achieve this we use the frequency shift key (FSK) feature of a commercial synthesiser that provides the frequency offsets with millihertz uncertainty. We then feed a low-pass-filtered version of the demodulated excitation signal to the synthesiser that controls the AOM before the reference cavity. This locks the frequency of the light sent to the comb (see Sect. 2.3) on the atomic Ramsey fringe centre (save for known fixed AOM offsets). Frequency offsets that can result from this modulation technique are discussed in Sect. 5.3.2.

For the evaluation of certain sources of frequency shifts (see Sect. 4), we use a second type of atomic interferometer, which is based on a photon echo pulse sequence [20, 31, 32]. This interferometer uses three time-separated pulses from one direction only (we refer to it as a symmetric AI) and is sensitive to phase rather than frequency. More specifically, the interferometer measures the difference in the average total phase accumulated by the atoms during each of the two dark periods, as can occur when atoms move through non-planar wave fronts of laser beams. To produce three-pulse interferograms, we sweep the phase of the first pulse relative to those of the last two. We achieve this by driving the phase/frequency offset AOM (Sect. 2.3 and Fig. 4) around the time of the first pulse from a synthesiser with its phase continuously modulated via an external modulation input. Before pulses 2 and 3 occur we switch to a second synthesiser with constant phase.

3 Calcium clock stability

3.1 *High-stability performance for the Ca standard*

We use the generated Ramsey fringes to determine the signal-to-noise ratio for the spectroscopic signals, and hence estimate the expected stability for the clock signals. The stability (as a function of averaging time) is important, since it tells us how long we need to average to reach a given level of precision. High levels of stability are one of the hallmarks of optical clocks since their line Q's can be much higher than those of their microwave counterparts [33]. Given a higher stability, we can evaluate potential clock shifts much more quickly. Figures 5a and 6 show excitation signals taken at different spectroscopic resolutions. Also shown is an estimate of the fractional frequency instability (for a 1-s averaging time) as a function of the FWHM width of the fringe. The lowest instability is achieved at a resolution between 500 and 900 Hz. At resolutions below 500 Hz the fringe contrast drops considerably, due to decay of the excited-state population (natural line width of the clock transition = 375 Hz [18]), while at resolutions above 1 kHz the reduced line Q degrades the stability. To confirm these stability estimates, we have performed external measurements against the Hg^+ frequency standard [24], by use of a femtosecond-laser comb to bridge the 76-THz frequency gap between the standards. The resulting frequency fluctuations showed a fractional frequency instability of 4×10^{-15} at 1 s, which averaged down to less than 2×10^{-16} at 2000 s [34].

Since it is experimentally convenient to work with a high signal-to-noise ratio, we typically operate at a resolution of 770 Hz, which is roughly the lowest resolution for which we still achieve the highest stability. We note that an instability of 4×10^{-15} at 1 s is competitive with the best demonstrated stability for any frequency standard, although it is still an order of magnitude larger than the quantum projection noise limit [33] for the number of atoms available in our apparatus.

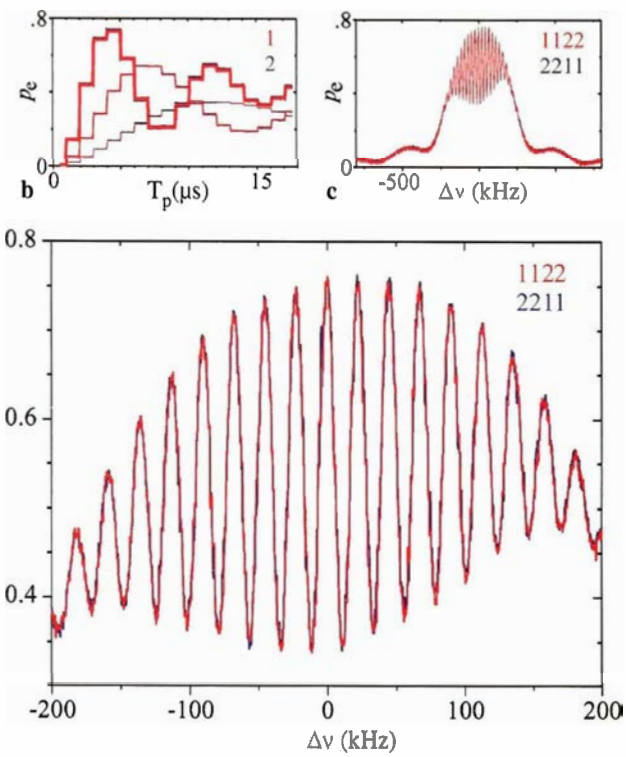

FIGURE 5 (a) A Bordé–Ramsey spectrum taken at a relatively low resolution of 11.55 kHz. The asymmetric envelope is a consequence of atomic recoil effects. (b) Rabi-flopping curve showing the degree of excitation as a function of the duration of the single probe pulse. For the highest Rabi frequency, two overlapped curves are shown, which were taken using beams from each of the two directions. This enables good matching of the two probe intensities. (c) Overlapped Bordé–Ramsey spectra taken with opposite pulse sequences. This shows that it made little difference from which direction the first pair of probe pulses originated

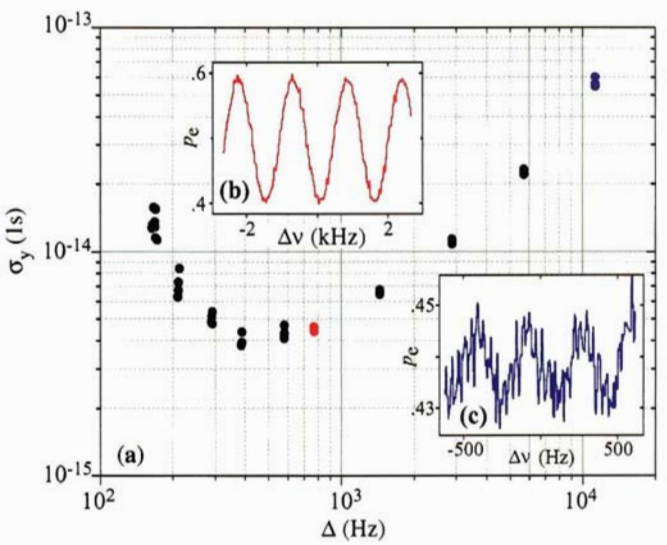

FIGURE 6 The *insets* show Bordé–Ramsey fringe patterns taken at resolutions of 770 Hz (b) and 180 Hz (c). Each spectrum is a 4-s frequency sweep containing single measurements at discrete frequencies. For the lowest resolution, see Fig. 5a. The data points in the main plot (a) show the fractional frequency instability for a 1-s averaging time as a function of resolution. The data are estimated from the scatter (rms values) on the fringe pattern

We have investigated the elevated noise level and now believe that it is due to frequency noise on the cavity-stabilised probe laser amplified by the optical Dick effect [35–37]. We have deduced the short-term noise of the free-running diode-laser system, i.e. stabilised to the stable cavity but not to the calcium clock transition, by beating the laser light against a comb line of the femtosecond laser system. The system was locked to the free-running laser system of NIST's Hg^+ frequency standard (see [24] for the short-term stability of this laser system). An approximate line width of less than 2 Hz at the calcium frequency standard's 456-THz frequency was measured on a time scale of 4 s, as well as a fractional frequency instability of $\sim 2 \times 10^{-15}$ at 1 s.

3.2 *Multiplexed signals for internal evaluations*

To expedite the evaluation of potential frequency biases in the Ca clock, we implemented a system that takes advantage of its high stability. The basic strategy for measuring such shifts is simply to change various experimental parameters with the laser locked to the central fringe and look for changes in the laser frequency. One technique we use is to compare measured frequencies to the Hg^+ system via the femtosecond laser comb. This approach is especially useful for parameters that can be changed only quite slowly, such as the Ca oven temperature (see Sect. 5.2.6). However, for parameters such as spectroscopic resolution that can be changed from one measurement cycle to the next ($\sim$ 25 ms), it is more convenient to use the short-term stability of the probe laser reference cavity for comparisons. For this purpose we constructed a multiplexed measurement system, which generates signals in parallel from alternate measurement cycles. The spectroscopic signals from the odd and even cycles are fed into two different electronic channels. We stabilise the laser to calcium in the usual way (see Sect. 2.1), except that we use only the odd measurement cycles. For the purpose of stabilisation this is similar to using 50-ms-long measurement cycles. In these odd cycles the system is run with one fixed set of experimental parameters. So, the laser frequency is locked to the calcium clock transition frequency including the systematic offset due to this set of parameters. In the even cycles a different set of parameters is used and the error signal measured with the laser frequency still set to the odd-cycle conditions. While in the odd cycles the error signal is zero on average due to the stabilisation, the offset measured in the even cycles reveals the systematic frequency shift between the two sets of experimental parameters. By referencing to the experimental parameters in the odd cycles, this alternating scheme allows us to take advantage of the high SNR of our system while simultaneously suppressing slow drifts in the experimental apparatus. In particular, the low drift rate of the reference cavity (compensated to yield an effective drift rate of less than 1 Hz/s) in conjunction with comparing the two experimental conditions every 25 ms, i.e. every cycle, yields an effective offset between the two signals of less than 50 mHz. The stability of the multiplexed measurement system enables hertz-level evaluations for an averaging time of 100 s.

4 A new approach for reducing residual first-order Doppler effects

The largest uncertainties in earlier Ca experiments [2, 20, 22, 32] were those resulting from imperfectly

cancelled first-order Doppler effects. These shifts result from the ballistic motion of the atoms in combination with imperfect probe laser collimation or overlap, or with non-orthogonality of the probe beams relative to gravity. The introduction of a second stage of laser cooling, which reduced atomic velocities by a factor of about 15, reduced these Doppler-related uncertainties considerably [10, 18, 27]. Here we describe a procedure that enables further reduction of the Doppler uncertainties by improving the characteristics of the probe beams themselves. This method is based on an idea by Trebst et al. [32], who showed how to use three- and four-pulse AIs to extract information about the probe laser beams. We have extended this method by performing the atomic interferometry with clouds of atoms launched at different velocities. Measuring phase and frequency shifts as a function of launch velocity enables isolation of the different laser beam imperfections. These features (wave-front curvature, mutual beam tilt, and orthogonality to the acceleration of gravity) can then be improved to reduce their contributions to the measurement uncertainty and their residual effects can be quantified.

The evaluation of the phase and frequency shifts was performed with the multiplexed measurement system described in Sect. 3. In this way we avoid the influence of phase-shifting contributions from other sources such as AOM frequency chirps (Sect. 5.3.1) due to common-mode rejection. The difference in offset phase (or frequency) for atomic interferograms taken with launched and unlaunched ensembles is measured by alternating between the two every 25 ms (every other cycle). This technique results in measured shifts of $\Delta\Phi = \Delta\Phi_{\text{launched}} - \Delta\Phi_{\text{unlaunched}}$ for three-pulse AIs and $\Delta\nu = \Delta\nu_{\text{launched}} - \Delta\nu_{\text{unlaunched}}$ for four-pulse AIs, respectively. Measuring these shifts as a function of launch velocity then provides the data used for probe beam characterisation.

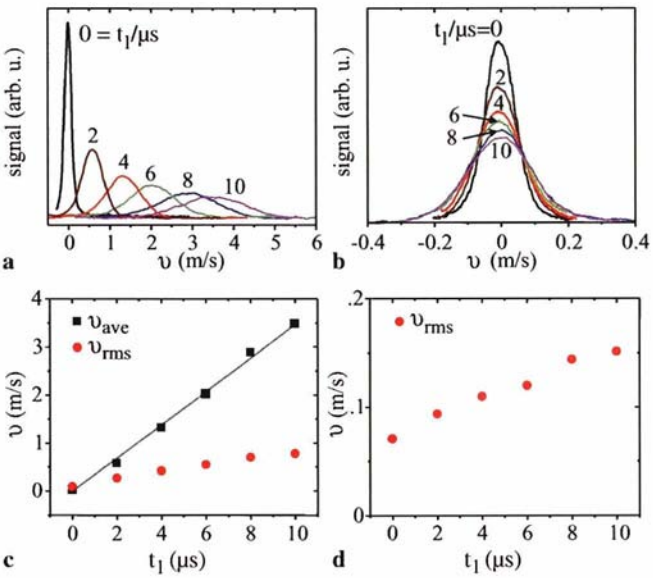

FIGURE 7 Summary of launching of the cold atom samples for leveraging systematic effects. (**a**) shows the velocity distributions in the direction of the launch (horizontal) as a function of time. (**b**) shows the velocity distributions in the perpendicular direction. (**c**) shows the measured launch velocities and rms velocities in the direction of the launch as a function of the duration of the launch pulse. (**d**) shows the much smaller increase in rms velocity along the probe beam direction (perpendicular to the launch)

4.1 *Launching atoms*

As we will see in the next few sections, the residual Doppler uncertainties of concern result from atom velocities that are *perpendicular* to the propagation direction of the probe beam. Thus, to take advantage of the launching technique to measure amplified versions of these effects, it is necessary to generate launches in two orthogonal directions perpendicular to the horizontal probe beam path. With our apparatus we launch atoms by applying near-resonant 423-nm laser pulses. For the perpendicular horizontal direction, we send launch pulses along the slowing beam direction. For studies in the vertical direction, we actually use launches at 45 degrees relative to the vertical due to restricted experimental access. With launching pulse durations of up to 16 μs, average velocities as large as 3 m/s can be achieved with rms broadening of the velocity as large as 90 cm/s along the launch direction and 20 cm/s perpendicularly. (Typical launched velocity distributions are depicted in Fig. 7.) The lower amount of broadening in the direction parallel to the probe beams (perpendicular to the launching direction) allows us to maintain high SNR in the atom interferograms.

4.2 *Wave-front curvature*

The first step of this procedure measures and minimises the wave-front curvature of each of the two probe beams (see Sect. 2.4) by comparing phase-dependent spectra based on symmetric three-pulse AIs. As the atoms move further out from the centre of the laser beam during the spectroscopic sequence, they sample a quadratically increasing offset from the wave-front surface for a non-planar (i.e. improperly collimated) laser beam. This motion produces a spatial phase chirp during the second dark period of the interferometer larger than that during the first, yielding a greater phase offset of the interferogram. In Fig. 9, examples are shown for phase-dependent interferograms with different launch velocities. Since the three-beam interferometer is also sensitive to gravitational acceleration, comparing launched and unlaunched ensembles separates the curvature effect (velocity sensitive) from the gravity effect (velocity insensitive). The phase-shift difference depends on the velocity, $v_{\text{launch},\perp}$, of the launched ensemble in the plane perpendicular to the k vector,

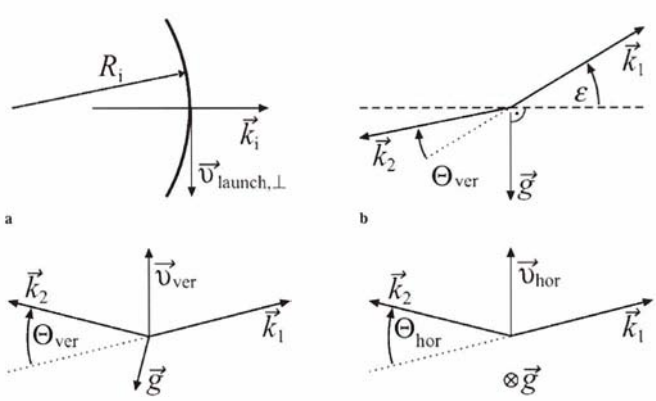

FIGURE 8 Sketch depicting the definition of the variables used for calculating the systematic Doppler effect: (**a**) for wave-front curvature, (**b**) for gravity contribution, (c) and (**d**) for vertical and horizontal mutual beam tilts

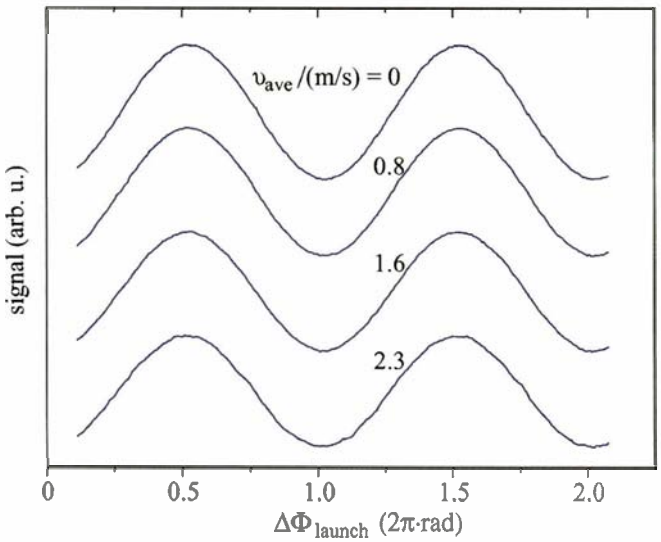

FIGURE 9 Interferograms resulting from the three-pulse AI sequence for four different cloud launching velocities. The interferograms slightly shift to the left with increasing launch velocity, indicating imperfect probe beam focusing as described in (1)

$\boldsymbol{k}$ (abs. value k), as well as on the radius of curvature, R_i, $i = 1, 2$, of the particular beam, and the interval between the laser pulses T (see [20, 32]):

$$\Delta\Phi = \frac{k}{R_i} v^2_{\text{launch},\perp} T^2 . \tag{1}$$

As depicted in Fig. 8, a positive R_i corresponds to a concave wave front along $\boldsymbol{k}$. Figure 10 shows the change in phase-shift difference as a function of launch velocity for three different resolutions. Initial offsets are presently not well understood, but are most likely due to oscilloscope sampling or to synchronised vibrations (see Sect. 5.3.3). By increasing the mean atom velocity, we amplify this shift considerably and correct it by adjusting the location of the collimating lens after the fibre that sets the location of the probe beam waist. Figure 10 also contains data showing the residual phase-shift sensitivity for a minimised wave-front curvature.

With the multiplexed AI signals our sensitivity of 10 mrad is sufficient to determine a probe beam radius of curvature of greater than 3000 m but, due to uncertainty in the laser beam quality (higher-order aberrations), the minimum radius of curvature was conservatively assigned a value of 200 m. For typical experimental drift velocities of 1.1 cm/s and a temperature of 11 μK, this yields shifts of less than 100 mHz at 770-Hz resolution. This corresponds to a relative uncertainty contribution of 2.2×10^{-16}. Assuming an improved beam quality where one would be limited only by the present sensitivity of the curvature measurement, the relative contribution could be as low as 2×10^{-17}.

4.3 *Mutual beam tilt*

Once the wave-front curvature is minimised, the frequency-sensitive, four-pulse AI can be used in combination with launching atoms to minimise the mutual beam tilt (i.e. the residual angle between the counterpropagating probe beams, Θ). The frequency shift $\Delta\nu_{\text{tilt},j}$, with j = (hor, ver) for the horizontal or vertical launch direction (Fig. 8), depends linearly on the product of the mutual angle, Θ_j, in the plane of the launch direction and the probe beams and the launch velocity, v_j [20, 32]:

$$\Delta\nu_{\text{tilt},j} \approx \frac{k\Theta_j}{8\pi} v_j . \tag{2}$$

The systematic shift is positive if the launch direction is parallel to the sum of the two $\boldsymbol{k}_i$. By comparing signals between launched and unlaunched atom clouds, we can minimise the resulting frequency shift by adjusting the beam alignment.

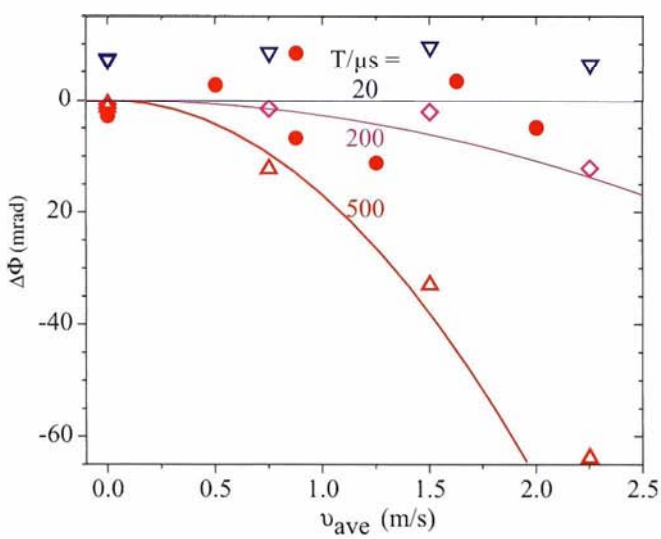

FIGURE 10 The sensitivity of phase difference measured with a symmetric AI to the launch velocity. The *open symbols* show measurements for a non-zero wave-front curvature of about 150 m. *Down-pointing triangles* are for a dark time of $T = 20$ μs, *diamonds* for 200 μs, and *triangles pointing up* for 500 μs, indicating the growing sensitivity with dark time. The *lines* show the theoretically expected shift for a radius of curvature of 150 m and the same dark times as used in the measurements. The *filled circles* represent a $T =$ 500 μs measurement after the wave-front curvature had been minimised

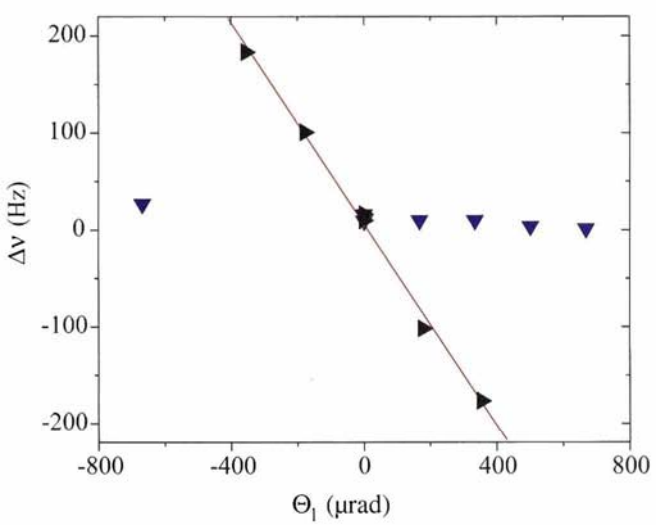

FIGURE 11 The four-pulse AI frequency shift as a function of mutual beam tilt (along the direction of the launch) for a launch velocity of 99 cm/s. The *down-pointing triangles* show that the signal is largely insensitive to mutual beam tilt perpendicular to the launch direction

However, this frequency shift is complicated by the fact that it also depends quadratically on the velocity in the product for wave-front curvature, and linearly on the velocity for an initial offset of the laser beams from the trap centre [20]. But, with the wave-front curvature already minimised and careful alignment to reduce the probe offset to less than 0.8 mm (for a laser beam with a waist of 3 mm and an atomic cloud with a rms radius of 2 mm), these effects limit the frequency uncertainty (for the launched atoms) at only the 6-Hz level. With launch velocities of nearly 1 m/s (and typical cloud drift velocities of ~ 1 cm/s), the frequency uncertainty due to the tilt can be reduced to around 50 mHz. Figure 11 shows measured frequency shifts as a function of mutual beam tilt for optimised wave-front curvatures. The tilt-minimisation procedure for our apparatus begins with a nulling in the horizontal direction with a launch velocity of ~ 60 cm/s and then in a diagonal direction ($\pi/4$ angle to the vertical) for a velocity of ~ 1.5 m/s (for the convenience of using the same launch time). The nulling of the frequency difference for launched vs. unlaunched atoms is accomplished by first adjusting the alignment to overlap the respective fringe patterns on an oscilloscope and to achieve a higher sensitivity by zeroing the error signal for the unlaunched ensemble condition while stabilising the laser to the launched atom condition. This can be accomplished with a 6-Hz uncertainty (determined by the noise in the detection process). Including the contributions of curvature, offset, and projection from the diagonal direction, the final uncertainty for the mutual beam tilt for the horizontal plane made up of the two probe beam k vectors is $u(\Theta_{\text{hor}}) = 16$ μrad and for the vertical plane $u(\Theta_{\text{ver}}) = 36$ μrad. From these values we determine a tilt-related shift of < 0.3 Hz for drift velocities up to 1.1 cm/s.

The uncertainties in Θ measured using beam-tilt-sensitive spectroscopy are consistent with a second approach where the coupling efficiency to the fibre of the opposite beam is used to minimise beam tilt. Based on geometric factors, this technique yields an uncertainty of 46 μrad, slightly larger than the net ~ 40 μrad for the launching procedure. We emphasise that the launching procedure was limited solely by the achievable laser beam curvature. With an optimised radius of curvature, and a 0.5-Hz sensitivity in measuring the frequency offset, a residual beam tilt of less than 1 μrad would be feasible. In that case the total residual Doppler uncertainty as outlined in [20] would be less than 7 mHz (relative uncertainty of 1.6×10^{-17}) for a 1-mm/s average velocity of the ensemble and use of the pulse-reversal technique (see Sect. 4.4).

4.4 *Gravity contributions*

Since the shift due to gravitational acceleration during the spectroscopy cannot be amplified by launching, a careful prealignment of the beams with respect to the tilt-stabilised optical table was carried out. With the other residual Doppler contributions already minimised, the angle-to-gravity effect can be directly measured by reversing the order of the pulses in the four-pulse AI, while keeping everything else the same. This gives a direct measure of the frequency shift, which is inversely proportional to the spectroscopic resolution [20, 32]. If we assume a situation as depicted in Fig. 8 with a small tilt of the k vector of beam 1 upwards from perpendicular to the direction of gravity, $\boldsymbol{g}$, with an angle ε, and correspondingly for the counterpropagating beam an angle $-\varepsilon + \Theta_{\text{ver}}$ (i.e. this beam is closer to perpendicular to $\boldsymbol{g}$ for $\Theta_{\text{ver}} > 0$), then we find for the beam order 1122

$$\Delta\nu_{g,1122} = \frac{g}{4\lambda}\left[-(T+2T_1)\varepsilon + (3T+2T_1+2T')(\varepsilon - \Theta_{\text{ver}})\right], \tag{3}$$

where T_1 is the time between switching off the trap and the first pulse and T' is the time between the two inner pulses. With a minimised mutual tilt we can assume that $\Theta_{\text{ver}} \ll \varepsilon$, and (3) can be approximated as $\Delta\nu_{g,1122} \approx (g/2\lambda)(T+T')\varepsilon$. This equation can be used to correct for the gravity contribution. Using pulse reversal with $\Delta\nu_{g,2211} = -\Delta\nu_{g,1122}$, the frequency difference for the two beam orders is

$$\Delta\nu_{\text{PR}} \approx \frac{g}{\lambda}(T+T')\varepsilon\,, \tag{4}$$

and allows us to directly extract ε from the pulse-reversal measurement. This procedure was carried out during frequency measurements and in internal measurements to correct the effect. A typical tilt-induced gravitational shift was 5 Hz at 770-Hz resolution, corresponding to $\varepsilon \approx 0.5$ mrad.

An alternative scheme could make use of averaging over the two beam sequences. With the beam order changed to 2211, ε and $(-\varepsilon + \Theta_{\text{ver}})$ would be swapped in (3). The frequency value would then be shifted due to the gravity contribution by

$$\frac{\Delta\nu_{g,2211} + \Delta\nu_{g,1122}}{2} = \frac{-g}{4\lambda}(2T+2T_1+T')\Theta_{\text{ver}}\,. \tag{5}$$

leaving only the angle of the mutual beam tilt in the vertical direction as a scaling factor for the gravity contribution, while the actual tilt to gravity would no longer contribute. To avoid effects of differences in the gains of the two error signals, the laser lock should alternate between the two different lock signals rather than average over the two error signals. However, with the present setup this approach could not be readily implemented. Finally, we are left with an uncertainty in Θ_{ver} that gives a contribution of 0.5 Hz (10^{-15}).

On the other hand, assuming an idealised situation as has been described in Sects. 4.2 and 4.3, the optimised wave-front quality would contribute to the fractional frequency with 2×10^{-17} and subsequently the mutual beam tilt with 1.6×10^{-17}. In this case and additionally alternating between the two pulse orders for locking as described above, the contribution due to gravity could effectively be reduced to well below 10^{-17}. Thus, the total fractional uncertainty of the residual Doppler effect could be reduced to well below 10^{-16}.

4.5 *Reproducibility*

Measurements of the minimised residual Doppler effect repeated over a five-day period indicate that the wave-front curvature, mutual beam tilt, and gravity contributions to systematic shifts stay within their respective levels of uncertainty over this period. This allows one to alternate between control and frequency measurements on a day to day basis and repeat part of the control measurements during the frequency-measurement days. The power in the pulses could drift within

a measurement day mainly due to coupling efficiency. They were monitored and the power did not change by more than 6% (see also Sect. 5.1).

Other important physical effects

With the residual first-order Doppler uncertainty reduced to the sub-hertz level, other important potential frequency shifts such as line-shape asymmetries and technical effects require more careful evaluation. Fortunately, isolating and measuring these various contributions is now much easier, since Doppler contributions no longer dominate measurements of clock shifts as a function of parameters such as resolution.

Asymmetry of the line shape

The recoil effect that is present in spectroscopy with ballistic atoms causes a fundamental asymmetry in the line shape produced by the frequency-dependent, four-pulse atom interferometer (see Fig. 5a) [30]. The asymmetric fringe envelope leads to shifts of the measured central fringe position, which depend on the stabilisation technique used. Taking into account measured velocity distributions, the ratio of probe beam diameter to atom cloud diameter, and laser intensities known from measurements of Rabi oscillations (see Fig. 5b), we performed simulations of the expected line shapes based on the formalism in [28]. The simulations allow us to compute the expected offset for the first-harmonic locking used in our setup (Sect. 2.4). In this locking scheme linear and higher-order terms added to the basically cosinusoidal line shape introduce an offset to the locking scheme. With probe pulse durations of 3 μs, the asymmetry contribution can be as large as 30 Hz for low resolution, where the fringe is spread out over a larger fraction of the asymmetric envelope as shown in Fig. 5a). Even at high resolution where the central fringe is only spread over a narrow region of the asymmetric envelope (see Fig. 6b), there is still a frequency offset of about 1 Hz at a 1-kHz resolution present. In Fig. 12 it can be seen that the sign of the offset changes with increasing resolution. This is due to the fact that in the Bordé–Ramsey scheme minima of the fringes occur at offsets of ± half the recoil splitting from line centre. With increasing resolution (increasing $T + T_p$) the number of periods between these minima increases and, hence, the sign of the cosinusoidal line shape of the centre fringe flips. With the laser stabilised to this central fringe, the sign of the gain of the harmonic locking is changed. Hence, the sign of the effect of the linear contribution in the asymmetry is changed.

Normally, we expect the frequency centre (although not the contrast) of the fringe pattern in the Bordé–Ramsey signal to be extremely insensitive to the intensities of the probe beams. However, the recoil-induced asymmetry adds a sensitivity to imbalances between the two beam intensities (the shift can even change sign) and, to a lesser degree, to overall intensity levels. To account for possible probe intensity drifts during the measurements, we allow for 6% intensity changes from those deduced from the measured Rabi oscillations to compute uncertainties for asymmetry-based corrections (see Fig. 12). Shorter pulse durations and the minimisation of dead time between the pulse pairs can reduce the effect of the asymmetry to below 100 mHz. With careful modelling and measurements of the actual spectroscopy parameters, corrections with a remaining uncertainty of 10% would allow us to compensate for the shift to better than 10 mHz (2×10^{-17}).

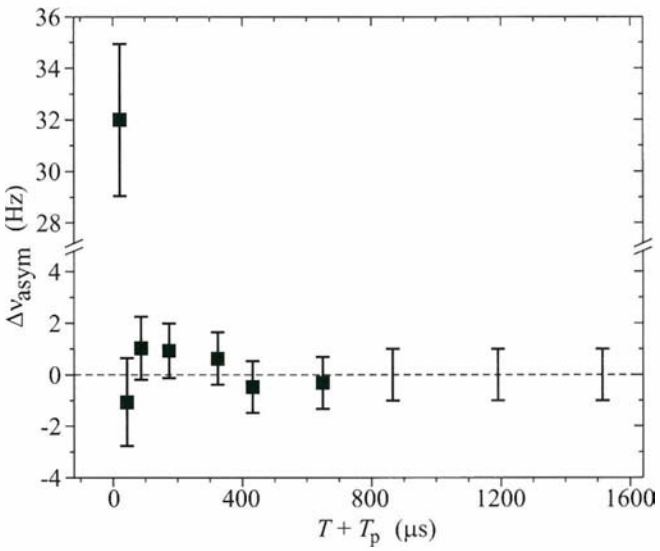

FIGURE 12 Computed line-shape-induced asymmetry shifts for experimental parameters measured from Rabi oscillations and velocity distributions. *Error bars* denote the range of shifts possible for a maximum change of intensity of 6% in either beam direction. The data are plotted for the resolutions used in the experiment, with 1, 2, 4, 8, 15, 20, 30, 40, 55, and 70 periods per recoil splitting. For the three highest resolutions only the uncertainties are indicated

5.2 *External fields*

5.2.1 AC Stark shifts. While the Ca clock transition is inherently extremely insensitive to stray electric and magnetic fields, stray light from the imperfectly extinguished laser cooling, quenching, or probe beams can lead to significant AC Stark shifts. In particular, the cooling and quenching lasers couple to transitions originating from the ground and excited-state energy levels of the clock transition. In a similar way the clock laser and the second-stage cooling laser couple to transitions involving the magnetically shifted Zeeman components of the $^3P_1$ excited state. In both cases, such couplings lead to intensity-dependent shifts of the measured clock frequency. To calculate the exact shifts we have included 19 transitions with their respective frequencies and oscillator strengths and calculated the possible total shifts from the maximum expected light intensities and laser frequencies. For the quenching transition where the actual oscillator strength is known only to within two orders of magnitude, we measured the AC Stark shift and extrapolated to lower intensities.

For our experimental apparatus AC Stark shifts are of particular concern, because the traditional method of using mechanical shutters to achieve high extinction ratios is not feasible, due to the short duration of the measurement cycle and the fast timing of the various pulses. Instead we use one or more AOM stages before the light beams are coupled to optical fibres, each yielding on/off extinction ratios ranging from 500 to 30 000, while maintaining the capability for fast switching of the beams.

For the 423-nm light, the three layers of AOM switches between the frequency-doubling cavity and the atom trap (Sect. 2.2) lead to a power extinction of $2.5 \times \mathbf{10^{-9}}$, yielding a total shift of less than 50 mHz. This level was verified by interlaced frequency measurements made with various switches intentionally left on.

Since the line strength of the 552-nm transition is not well known, we needed to make more direct measurements of potential shifts due to leakage of the quenching laser light. Thus, we performed frequency measurements at low spectroscopic resolution with the full quenching power incident on the atomic ensemble. As we scanned the green laser frequency over the quenching transition resonance, we measured the induced shift of the clock laser frequency. Figure 13 shows the resulting frequency shift. A frequency shift of less than 2500 Hz on the clock transition was measured for the full incident power. Taking into account the AOM extinction ratio of 3×10^{-5} leaves a maximum shift of less than 85 mHz. During the Ca frequency measurements the power was reduced by an additional factor of five, yielding a shift of less than 20 mHz (4×10^{-17}, fractionally).

An AC Stark shift due to the red laser can result from interactions with the Zeeman components of the $^3P_1$ state that cause shifts of the ground states. With the multiple AOM stages the red-light leakthrough for cooling and probe beams leads to shifts of less than 1 mHz. The shift due to off-resonant excitation for higher-lying levels is less than 1.5 mHz for a typical probe intensity of 30 mW/cm^2.

5.2.2 Quadratic Stark shift. DC electric fields due to patch potentials on the surface of the stainless steel vacuum chamber with a distance ≥ 3 cm from the trapped atoms can cause a quadratic Stark shift due to differential polarisability of the ground and excited states. DC field gradients are assumed to lie with equal probability in the (very conservatively) chosen range of ± 200 V/m and with fields of arbitrary polarisation. With the resulting differential polarisability of $\Delta\alpha = (3.07 \pm 0.06)\ \mu\text{Hz(V/m)}^2$ [38, 39] the possible shift is less than 70 mHz and is included as an uncertainty contribution.

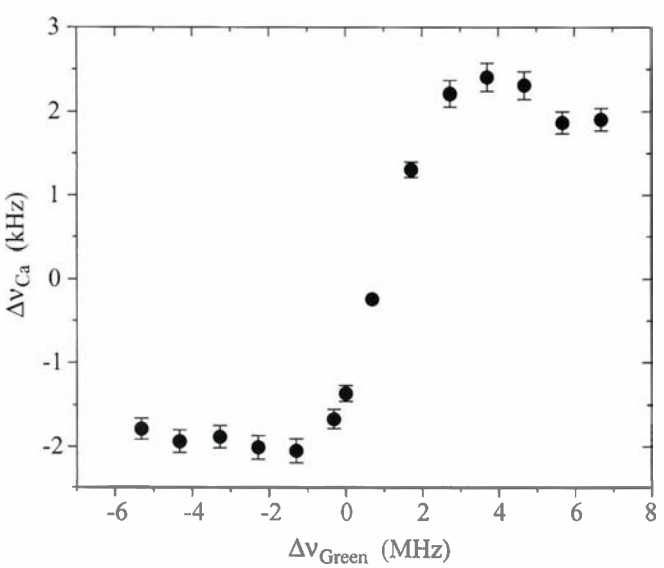

FIGURE 13 Stark shifts of the clock transition as a function of 552-nm laser detuning from the normal setting for second-stage cooling with the green light intentionally left on. The green light beam passes through the trap four times with a waist of ~ 1.5 mm and a power of ~ 90 mW. Under normal clock conditions, the intensity of the 552-nm light (and the induced light shift) is reduced by a factor of more than 30 000

5.2.3 Black-body shift. For this system there are two potential sources of black body radiation induced clock shifts. The first originates from the room-temperature environment surrounding the atomic cloud, while the second comes from the oven (800 to 900 K), located 13 cm from the trap centre. We can estimate these shifts using the DC value for the atom polarisability, since the peak of the black-body radiation lies far from the wavelengths of the relevant transitions ($< 2\ \mu$m). A more exact method by Farley and Wing [40] yields values that differ by less than 15% from the DC values [10]. For the room-temperature contribution, we include a 5-K temperature spread due to uncertainty in the effect of the water-cooled high-current quadrupole coils attached to the vacuum chamber. Using the known values for the differential DC polarisability, we find a shift of 1.01 ± 0.07 Hz for a temperature of 295 ± 5 K.

Estimating the contribution of the Ca oven is somewhat more difficult. The oven has a temperature ranging from 800 to 900 K and an effective aperture of 0.5-cm radius and is enclosed in a water-cooled housing. The housing has a maximum temperature of 600 K and a radius of 2.3 cm. The oven assembly is 13 cm away from the trap but the high reflectivity of the metal tube connecting the oven and main chamber could function as a fibre-like connector, effectively increasing the fraction of radiation making it to the atom cloud. For conservative parameters, we estimate a maximum frequency shift of -200 mHz, but it is likely much closer to zero. Rather than make a correction, we have added a 200-mHz contribution to the total uncertainty budget.

5.2.4 Second-order Zeeman shift. The π component of the clock transition has no linear magnetic field dependence and only a very small second-order Zeeman-shift coefficient of $(+63.75 \pm 0.09)$ MHz/T^2. A diamagnetic contribution from the clock ground state can be assumed to be less than 1% of this coefficient [41]. The combined effect has been measured by different groups [21, 38, 41, 42] and was found to be $(+64 \pm 1)$ MHz/T^2. The linear magnetic shifts of the σ components relative to the π transition of ± 21.0 GHz/T [42] can be used to measure the value of the magnetic field at the location of the atoms. During clock operation a typical measured field is $(151 \pm 30)\ \mu$T, resulting in a shift of $(+1.47 \pm 0.07)$ Hz.

5.2.5 Density-dependent frequency shifts. At PTB measurements of the density-dependent frequency shift due to collisions between Ca atoms at a temperature of about 20 μK were made. These measurements were made with densities ranging from about 10^{14} /m^3 to 1.2×10^{16} /m^3. Assuming that the frequency shift scales linearly with density, it was found that the frequency-shift coefficient was consistent with zero to within $\varrho \times 7.3 \times 10^{-17}$ Hz m^3, where ϱ is the cold atom density [10]. Due to the short cycle times and the lack of trapping in the second-stage cooling, the number densities in the NIST setup

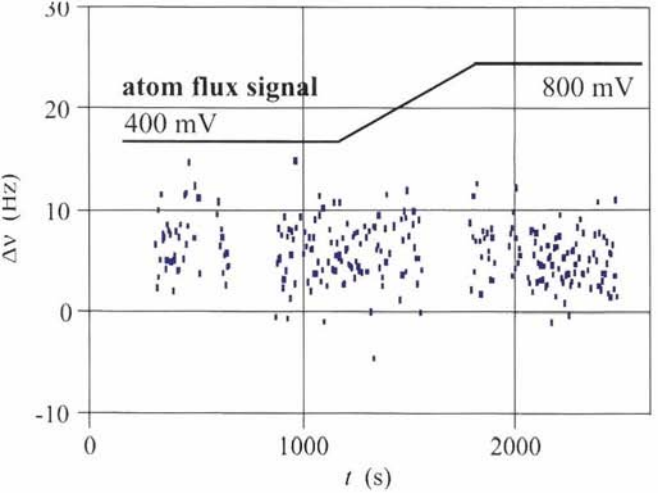

FIGURE 14 Frequency comparison (arbitrary offset, 10-s averages) between the single-ion mercury clock and the calcium optical frequency standard with two different atomic beam fluxes set by oven temperature. Initial and final fluxes including the intermediate range where the oven temperature was changed are indicated

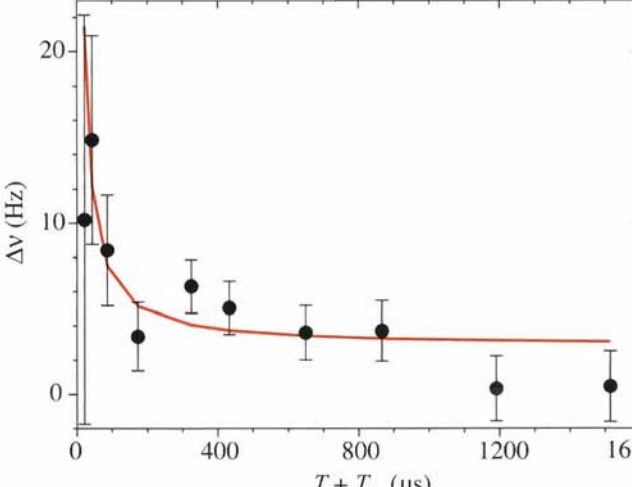

FIGURE 15 The shift in the Ca clock frequency as a function of T, dark period for each pair of Bordé–Ramsey pulses, measured using multiplexed system. After accounting for the contribution of the line-sha asymmetry, we find the expected $1/T$ dependence (the *line* shows a weigh fit to the data) that would result from AOM phase chirps. This leads to a c rection of 1.6 Hz at the working resolution of 770 Hz ($T + T_p = 324$ μs)

were below 10^{14} /m^3, with a corresponding uncertainty in the frequency shift of 10 mHz.

5.2.6 Collisions with thermal atoms. Since the fast atoms in the thermal beam impinge directly on the laser-cooled cloud, there exists a possibility for significant shifts resulting from collisions between fast and slow atoms. To search for such effects we varied the temperature of the Ca oven, thereby changing the flux of fast atoms, which was calibrated with a detection beam aligned perpendicular to the atomic beam. Frequency measurements were made against calibrated hydrogen masers from the NIST time scale as we varied the flux by a factor of three. Note that we could not measure relative to the cavity because the oven takes 10 to 20 min to settle at a new temperature. A first set of measurements showed a shift of less than 2 Hz, limited by the stability of the maser. A subsequent measurement against the Hg^+ frequency standard was performed. The flux of atoms was varied by a factor of two. Figure 14 shows the results of the measurement of the change in frequency offset. A slow drift is likely due to the effect of synchronised vibrations slowly changing over time (Sect. 5.3.3) and does not show any correlation with the change in flux also indicated in the figure. From the measurement an upper bound of -0.9 ± 2.2 Hz for the shift due to atomic flux can be given that confirms the maser results.

5.2.7 Relativistic Doppler shift. For the low velocities in the microkelvin ensemble the relativistic Doppler shift can be approximated to second order, resulting in $\Delta\nu_{RD} = -\nu_{Ca} \times (v_{rms}^2/2c_0^2)$. This shift is well below 20 μHz for ensemble temperatures of up to 15 μK.

5.3 *Technical effects*

5.3.1 Phase shifts originating from pulse switching. An im-

from the short light pulses used to excite the atoms. Wh the brevity (3 μs) of these pulses leads to high-contrast si nals, it also makes the pulses very sensitive to rf phase shi and chirps. These phase deviations are caused by transient e fects in the rf switching and AOMs as the signal is fed throu a rf amplifier to the AOM resonant circuit. When the pha deviations are imprinted onto the laser light, they can le to shifts of the Bordé–Ramsey fringe patterns used for s bilisation. For a detailed treatment and investigation of the effects, see [43]. This effect scales linearly with the resoluti (or, equivalently, inversely with the time interval between t pulses). After applying the independently deduced corre tions for other resolution-dependent effects, this systema shift can be explicitly measured and subsequently compe sated. In Fig. 15 the measured phase-chirp effect is show including a fit to a $1/T$ dependence, and indicates a shift about 1.6 Hz with an uncertainty of 0.9 Hz at the 'norm resolution of 770 Hz. The data shown here were measur internally with the multiplexed measurement system and a consistent with external measurements of this shift against t Hg^+ clock.

5.3.2 Electronic offsets. Potential electronic offsets in t laser locking system are reduced by the purely integrati nature of the feedback loop used to lock the laser to the transition. Measurements of offsets in the electronics lead estimates of less than 0.1% of the spectroscopic line wi and are included in the uncertainty budget. For measureme at the 1-Hz level it is also necessary to evaluate potent electronic offset shifts resulting from residual laser drift. D to imperfect stabilisation of the temperature of the housi that contains the reference resonator, the free running las drift can be as large as 10 Hz/s, but can be reduced w a manually adjusted linear feedforward to below 1 Hz/s. be able to calculate the corresponding shift due to the s gle integrating stage of the stabilisation [38, 44] the ser

siser used for the offset between reference resonator and calcium transition was stepped rapidly to achieve a probe laser frequency step of typically a quarter of the resolution used for stabilisation. Simultaneously, the servo error and correction signals were recorded. Figure 16 shows the resulting signals for the lowest, normal, and highest resolutions used, along with the measured time constants for the different resolutions.

At the standard (770-Hz) resolution, the correction time constant is 50 ms, corresponding to the combined duration of the two measurement cycles necessary for the $1f$ stabilisation scheme. The time constants are several times longer for the highest and lowest resolutions, due to reduced stability of the spectroscopic signal. The short servo attack times allow us to keep the systematic shift due to a maximum linear free running laser drift of 1 Hz/s to below 800 mHz for the low-stability case and below 100 mHz for resolutions between 500 Hz and 1 kHz.

5.3.3 Synchronised vibrations. One source of systematic error for these measurements resulted from vibrations induced in the optical table when the quadrupole coils for the magneto-optic trap were turned on and off. Since the reference resonator providing the short-term stability of the clock laser was originally located on the same (floating and actively levelled) optical table, vibrations were coupled through the table from the coils to the cavity. The switching of the coils excited resonances between 0.3 and 2 kHz in the overall mechanical setup that combined into a waveform for the acceleration of the optical table. Measurements with an accelerometer triggered off the frequency standards measurement cycle and averaged over extended numbers of cycles showed a fixed phase relationship and negligible change in waveform and amplitude up to hours. Changes in the total duration of the measurement cycle and/or changes of the position of the quadrupole switching within this cycle did change the waveform, but were reproducible. Since acceleration of the reference resonator induces proportional variation in the resonator length, the probe laser frequency was modulated proportionally to the acceleration and this modulation was synchronised with the measurement cycle. The absolute laser stabilisation in turn was based on a comparison of the laser frequency to the atomic transition frequency during 1 ms in the 25-ms measurement cycle. This led to a fixed offset of the stabilised laser frequency averaged continuously in frequency measurements against the mercury frequency standard or the caesium atomic clock. This fixed offset was a function of when the excitation sequence occurred in the cycle, i.e. which part of the acceleration/frequency offset waveform was sampled while comparing to the clock transition. Shifts as large as tens of hertz were seen.

To reduce this sensitivity, we decoupled the vacuum system from the optical table by suspending it just above the table with an outside support. A set of multiplexed measurements with variable time delays added to the end of each cycle (in 10-μs steps up to several 100 μs) verified that this effect was suppressed with a 1-Hz uncertainty. In this way we did not change any other systematic in the measurement cycle. We only changed the acceleration waveform by waiting different times before the next measurement cycle started. The level of uncertainty was verified by a second set of measurements that used the Hg^+ standard as a reference. In this case we took 100-μs steps from zero delay up to 2 ms, and found a standard deviation of 1.1 Hz for the scatter of the frequency values, which we took as the contribution to the total uncertainty. Note that these effects could also contribute to limitations in systematic uncertainties in the resolution-dependent measurements (see Sect. 5.3.1 and Sect. 5.1).

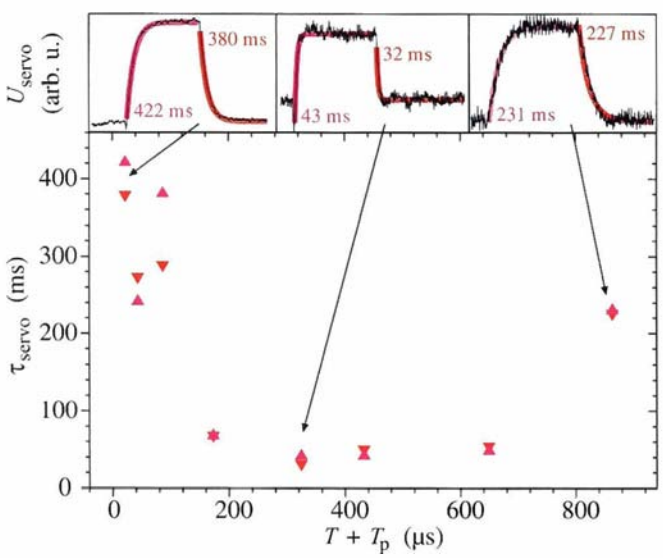

FIGURE 16 The temporal response of the stabilisation loop to artificial frequency steps for several different Ramsey dark times with $T_p = 3\,\mu s$

6 Total uncertainty for the calcium standard

In Table 1, which summarises the measured frequency shifts and their contributions to the total uncertainty (all reported uncertainties are 1σ), two results stand out. First, the net frequency shift of the laser locked to the spectroscopic signal from the unperturbed Bohr frequency is small (−3.27 Hz), so we are not in the uncomfortable position of having to make large corrections at an extremely fine level. Second, the resulting total uncertainty is 3.03 Hz for the system, which represents an improvement by a factor of more than six over our previous result from 2000 [2, 22]. The 2000 result was based on calcium samples with temperatures of a few mK rather than 10 μK. Indeed, the dominant contributor to the millikelvin atom-based uncertainty was the first-order Doppler effect, which motivated the two-pronged approach adopted here (second-stage laser cooling and improvement of the laser beams through atom interferometry with launched clouds of atoms). We note that a more recent measurement of the calcium transition frequency at PTB achieved an uncertainty of 5.3 Hz, with 4.3 Hz resulting from uncertainty in the calcium standard itself [18]. This measurement also benefited from a second stage of laser cooling (resultant temperature ~ 10 μK), although a different quenching transition was used [16].

With the uncertainty of our standard reduced to 3 Hz, it is of considerable interest to measure its absolute frequency and compare it to previous measurements. Such a measurement has been performed and soon will be reported elsewhere.

Effect	$\Delta\nu_{Ca}$ (Hz)	$u(\Delta\nu_{Ca})$ (Hz)
Residual Doppler	−4.7	0.9
Asymmetry	0.3	1.0
Other phase shifts	1.6	0.8
Magnetic field	1.47	0.07
Quadratic Stark	−0.03	0.02
Black body (room)	−1.01	0.07
Black body (oven)	0	0.2
AC Stark	0	0.1
Cold collisions	0	0.011
Thermal atoms (oven)	−0.9	2.2
Synchronized vibrations	0	1.1
Electronic offsets	0	0.8
Ca total	−3.27	3.03

TABLE 1 Uncertainty budget for the Ca standard for a spectroscopic resolution of 770 Hz (see text for details). $\Delta\nu_{Ca}$ is the shift (i.e. the applied correction to the final frequency value) due to a particular effect and $u(\Delta\nu_{Ca})$ is its uncertainty

7 Future prospects for the calcium standard

One encouraging aspect of Table 1 is that the total uncertainty is dominated by a variety of technical effects (rather than by fundamental physical limitations), several of which can easily be addressed. Specifically, the uncertainty associated with possible collisions with fast atoms in the atomic beam can be greatly reduced by the introduction of a beam block (e.g. with a thin wire placed in the atomic beam to make a shadow around the trapped atoms). Alternatively, we can locate the magneto-optic trap outside the beam path by using an optical molasses arranged at an angle to send atoms from the beam to the trap only during the trap-loading cycle [45]. The second largest contributor, the uncertainty due to synchronised vibrations between the quadrupole coils and the reference cavity, will be suppressed simply by relocating the cavity on a different table (linked by a Doppler-cancelled fibre connection [46]). While we will still need to check for possible synchronised vibrations of the optical elements on the table, this effect should be greatly reduced. Reduction of these two main contributors would lower the net uncertainty to 1.8 Hz.

Further reduction in the uncertainty is still possible, since the key remaining contributors are also technical in nature and could be addressed in future versions.

In fact, measurements at levels $< 10^{-15}$ seem feasible. The low 10^{-16} range might even be achieved, if the technical issues associated with the AOM phase chirps can be overcome and asymmetry shifts can be reliably modelled at the appropriate level. Additionally, since several of the critical issues for the Ca standard (AOM-related shifts, asymmetry shifts) are resolution dependent, going to higher resolution would be advantageous. Although a significant increase in resolution is not practical for the 657-nm transition ($^1S_0 - {}^3P_1$) used here (due to its 375-Hz natural line width [18]), the 70-Hz-wide transitions at 457 nm in Ca ($^1S_0 - {}^1D_2$) or Mg ($^1S_0 - {}^3P_1$) could provide attractive alternatives. However, we quickly run into another limit here due to the ballistic nature of the freely expanding atoms, namely, the acceleration due to gravitation, which effectively limits interaction times to roughly 30 ms. A further increase in resolution could result from a fountain geometry similar to that used for Cs primary standards, but this is more difficult to implement in the optical domain. In any case, significant atomic motion through the laser beams will severely challenge the wave-front quality of the probe laser beams independent of choice of atom and narrow clock transition.

The great advantage of these frequency standards is their potential to reach unprecedented stability on timescales as short as 10 ms. Experimental data show that an improved overlap the respective zero points of the magnetic quadrupole fields for the two cooling stages could allow second stage cooling times as low as 4 ms. An increased cooling beam diameter for the second-stage cooling could improve the transfer efficiency and an increased loading rate, e.g. by the use of a Zeeman slower, would allow us to shorten the reloading and first-stage cooling time possibly to 4 ms or less. A narrow microkelvin velocity distribution with about 10^7 well-localised atoms could be achieved in 10 ms, thus allowing a 100-Hz repetition rate without compromise on the projected uncertainty budget. At the same time, this would allow one to relax the specifications for the prestabilised clock laser to achieve a minimised contribution through the Dick effect on the stability budget.

8 Conclusions

We have presented a detailed investigation of the potential shifts for the calcium frequency standard based on freely expanding atoms cooled to microkelvin temperatures. To investigate the shifts efficiently, we constructed a multiplexed measurement scheme that took advantage of the high stability of the standard (4×10^{-15} at 1 s). This system enabled internal evaluations of the majority of the critical shifts (relative to a high-finesse resonator). With the use of microkelvin atoms, a total uncertainty of 3.3 Hz was demonstrated with good prospects for sub-hertz performance.

Of particular importance in this work was the development of a new scheme for improving the laser probe beam parameters through atom interferometry with launched clouds of microkelvin atoms. This method could be applied to precision experiments involving freely expanding atoms and can potentially reduce first-order Doppler effects to less than one part in 10^{16}, assuming adequate beam quality. Achieving a total uncertainty at this level will probably require the use of a narrower transition as well as careful evaluation and control over several other effects. Eventually, it could turn out that the most accurate optical standards based on neutral atoms will result from lattice-based systems [9], which can confine atoms in a Doppler-free environment, thereby largely removing Doppler-related issues (wave-front curvature, beam quality, beam alignment, and AOM shifts) from the uncertainty budget. However, due to their relative simplicity in comparison with their trapped-ion and lattice-based counterparts, clocks based on freely expanding atoms will likely find many applications, especially those for which high stability is the critical factor.

ACKNOWLEDGEMENTS We thank Joe Wells and the Alexander von Humboldt Foundation for their support of G. Wilpers during his time at NIST.

REFERENCES

1 T. Udem, J. Reichert, R. Holzwarth, T.W. Hänsch, Opt. Lett. **24**, 881 (1999)
2 T. Udem, S.A. Diddams, K.R. Vogel, C.W. Oates, E.A. Curtis, W.D. Lee, W.M. Itano, R.E. Drullinger, J.C. Bergquist, L. Hollberg, Phys. Rev. Lett. **86**, 4996 (2001)
3 S.A. Diddams, D.J. Jones, J. Ye, S.T. Cundiff, J.L. Hall, Phys. Rev. Lett. **84**, 5102 (2000)
4 L.S. Ma, Z. Bi, A. Bartels, L. Robertsson, M. Zucco, R.S. Windeler, G. Wilpers, C. Oates, L. Hollberg, S.A. Diddams, Science **303**, 1843 (2004)
5 S.A. Diddams, J.C. Bergquist, S.R. Jefferts, C.W. Oates, Science **306**, 1318 (2004)
6 H.S. Margolis, G.P. Barwood, G. Huang, H.A. Klein, S.N. Lea, K. Szymaniec, P. Gill, Science **306**, 1355 (2004)
7 E. Peik, B. Lipphardt, H. Schnatz, T. Schneider, C. Tamm, S.G. Karshenboim, Laser Phys. **15**, 1028 (2005)
8 W.H. Oskay, S.A. Diddams, E.A. Donley, T.M. Fortier, T.P. Heavner, L. Hollberg, W.M. Itano, S.R. Jefferts, M.J. Delaney, K. Kim, F. Levi, T.E. Parker, J.C. Bergquist, Phys. Rev. Lett. **97**, 020801 (2006)
9 M. Takamoto, F.L. Hong, R. Higashi, H. Katori, Nature **435**, 321 (2005)
10 U. Sterr, C. Degenhardt, H. Stoehr, C. Lisdat, H. Schnatz, J. Helmcke, F. Riehle, G. Wilpers, C.W. Oates, L. Hollberg, C.R. Physique **5**, 845 (2004)
11 M. Fischer, N. Kolachevsky, M. Zimmermann, R. Holzwarth, T. Udem, T.W. Hänsch, M. Abgrall, J. Grünert, I. Maksimovic, S. Bize, H. Marion, F.P.D. Santos, P. Lemonde, G. Santarelli, P. Laurent, A. Clairon, C. Salomon, Phys. Rev. Lett. **92**, 230802 (2004)
12 F. Ruschewitz, J.L. Peng, H. Hinderthür, N. Schaffrath, K. Sengstock, W. Ertmer, Phys. Rev. Lett. **80**, 3173 (1998)
13 K.R. Vogel, T.P. Dinneen, A. Gallagher, J.L. Hall, IEEE Trans. Instrum. Meas. **48**, 618 (1999)
14 H. Katori, T. Ido, Y. Isoya, M. Kuwata-Gonokami, Phys. Rev. Lett. **82**, 1116 (1999)
15 E.A. Curtis, C.W. Oates, L. Hollberg, Phys. Rev. A **64**, 031403(R) (2001)
16 T. Binnewies, G. Wilpers, U. Sterr, F. Riehle, J. Helmcke, T.E. Mehlstäubler, E.M. Rasel, W. Ertmer, Phys. Rev. Lett. **87**, 123002 (2001)
17 E.A. Curtis, C.W. Oates, L. Hollberg, J. Opt. Soc. Am. B **20**, 977 (2003)
18 C. Degenhardt, H. Stoehr, C. Lisdat, G. Wilpers, H. Schnatz, B. Lipphardt, T. Nazarova, P.-O. Pottie, U. Sterr, J. Helmcke, F. Riehle, Phys. Rev. A **72**, 062111 (2005)
19 T. Ido, T.H. Loftus, M.M. Boyd, A.D. Ludlow, K.W. Holman, J. Ye, Phys. Rev. Lett. **94**, 153001 (2005)
20 G. Wilpers, C. Degenhardt, T. Binnewies, A. Chernyshov, F. Riehle, J. Helmcke, U. Sterr, Appl. Phys. B **76**, 149 (2003)
21 C.W. Oates, F. Bondu, R.W. Fox, L. Hollberg, Eur. Phys. J. D **7**, 449 (1999)
22 E.A. Curtis, Quenched narrow-line laser cooling of ^{40}Ca with application to an optical clock based on ultracold neutral Ca atoms. Tech. Rep., National Institute of Standards and Technology, Boulder, CO, USA; Dissertation, University of Colorado, Boulder (2003)
23 T. Kurosu, F. Shimizu, Japan J. Appl. Phys. **31**, 908 (1992)
24 B.C. Young, F.C. Cruz, W.M. Itano, J.C. Bergquist, Phys. Rev. Lett. **82**, 3799 (1999)
25 L. Hollberg, S.A. Oates, A. Bartels, T. Fortier, K. Kim, Metrologia **42**, 2037 (2005)
26 W.M. Itano, J.C. Bergquist, J.J. Bollinger, J.M. Gilligan, D.J. Heinzen, F.L. Moore, M.G. Raizen, D.J. Wineland, Phys. Rev. A **47**, 3554 (1993)
27 G. Wilpers, T. Binnewies, C. Degenhardt, U. Sterr, J. Helmcke, F. Riehle, Phys. Rev. Lett. **89**, 230801-1 (2002)
28 C.J. Bordé, C. Salomon, S. Avrillier, A. Van Lerberghe, C. Bréant, D. Bassi, G. Scoles, Phys. Rev. A **30**, 1836 (1984)
29 C.J. Bordé, Phys. Lett. A **140**, 10 (1989)
30 C.W. Oates, G. Wilpers, L. Hollberg, Phys. Rev. A **71**, 023404 (2005)
31 Y. Omi, A. Morinaga, Appl. Phys. B **67**, 621 (1998)
32 T. Trebst, T. Binnewies, J. Helmcke, F. Riehle, IEEE Trans. Instrum. Meas. **50**, 535 (2001)
33 L. Hollberg, C.W. Oates, E.A. Curtis, E.N. Ivanov, S.A. Diddams, T. Udem, H.G. Robinson, J.C. Bergquist, R.J. Rafac, W.M. Itano, R.E. Drullinger, D.J. Wineland, IEEE J. Quantum Electron. **QE-37**, 1502 (2001)
34 L. Hollberg, C.W. Oates, G. Wilpers, C.W. Hoyt, Z.W. Barber, S.A. Diddams, W.H. Oskay, J.C. Bergquist, J. Phys. B **38**, 469 (2005)
35 G.J. Dick, J. Prestage, C. Greenhall, L. Maleki, Local oscillator induced degradation of medium-term stability in passive atomic frequency standards. In *Proc. 22nd Annu. Precise Time and Time Interval (PTTI) Applications and Planning Meet.*, Vienna, VA, USA, 1990, pp. 487–509
36 G. Santarelli, C. Audoin, A. Makdissi, P. Laurent, G.J. Dick, A. Clairon, IEEE Trans. Ultrason. Ferroelectr. Freq. Control **45**, 887 (1998)
37 A. Quessada, R. Kovacich, I. Courtillot, A. Clairon, G. Santarelli, P. Lemonde, J. Opt. B **5**, S150 (2003)
38 G. Zinner, Ein optisches Frequenznormal auf der Basis lasergekühlter Calciumatome. PTB-Bericht PTB-Opt-58, Physikalisch-Technische Bundesanstalt, Braunschweig (1998)
39 K. Zeiske, Atominterferometrie in statischen elektrischen Feldern. PTB-Bericht PTB-Opt-48, Physikalisch-Technische Bundesanstalt, Braunschweig (1995)
40 J.W. Farley, W.H. Wing, Phys. Rev. A **23**, 2397 (1981)
41 N. Beverini, E. Maccioni, F. Strumia, J. Opt. Soc. Am. B **15**, 2206 (1998)
42 N. Beverini, F. Strumia, High precision measurements of the Zeeman effect in the calcium metastable states. In *Interaction of Radiation with Matter, A Volume in Honour of A. Gozzini* (Quaderni della Scuola Normale Superiore de Pisa, Pisa, 1987), pp. 361–373
43 C. Degenhardt, T. Nazarova, C. Lisdat, H. Stoehr, U. Sterr, F. Riehle, IEEE Trans. Instrum. Meas. **54**, 771 (2005)
44 G. Wilpers, Ein Optisches Frequenznormal mit kalten und ultrakalten Atomen. PTB-Bericht PTB-Opt-66, Physikalisch-Technische Bundesanstalt, Braunschweig [ISBN 3-89701-892-6]; Dissertation, University of Hannover (2002)
45 T. Kisters, K. Zeiske, F. Riehle, J. Helmcke, Appl. Phys. B **59**, 89 (1994)
46 L.S. Ma, P. Jungner, J. Ye, J.L. Hall, Opt. Lett. **19**, 1777 (1994)